materials

MDPI

Article

Efficient Green Synthesis of (Fe_3O_4) and ($NiFe_2O_4$) Nanoparticles Using Star Anise (*Illicium verum*) Extract and Their Biomedical Activity against Some Cancer Cells

Noha Al-Qasmi [1,*], Fahad A. Almughem [2], Somayah J. Jarallah [2] and Amani Almaabadi [2,*]

[1] Chemistry Department, Faculty of Science, Taif University, Al Hawiyah, P.O. Box 11099, Taif 21944, Saudi Arabia
[2] National Center for Biotechnology, Life Science and Environment Research Institute, King Abdulaziz City for Science and Technology (KACST), Riyadh 11442, Saudi Arabia; falmughem@kacst.edu.sa (F.A.A.); sjarallah@kacst.edu.sa (S.J.J.)
* Correspondence: noha.alqasmi@tu.edu.sa (N.A.-Q.); aalmaabadi@kacst.edu.sa (A.A.)

Abstract: Magnetite Fe_3O_4 and spinel (2:1) and (4:1) $NiFe_2O_4$ magnetic nanoparticles (MNPs) were prepared by simple and affordable co-precipitation methods using an extract of star anise (*Illicium verum*) as a green reducing agent. The morphology and chemical composition of these MNPs were confirmed by field-emission scanning electron microscopy, energy-dispersive X-ray spectroscopy, UV–visible spectroscopy, and X-ray diffraction (XRD). The synthesized magnetite Fe_3O_4 and spinel (2:1) and (4:1) $NiFe_2O_4$ MNPs were in the size range of 0.1–1 µm. The MNPs had irregular clustered platelets (magnetite Fe_3O_4) and pyramidal structures (spinel (2:1) and (4:1) $NiFe_2O_4$ NPs). The average sizes of the synthesized magnetite Fe_3O_4, and spinel (2:1) and (4:1) $NiFe_2O_4$ MNPs calculated using XRD analysis were 66.8, 72.5, and 72.9 nm, respectively. In addition to the characteristic absorption peaks of magnetite Fe_3O_4, those of spinel (2:1) and (4:1) $NiFe_2O_4$ MNPs were detected at ~300–350 nm and ~700 nm, respectively. Overall, the results of this study indicate that the synthesized magnetite Fe_3O_4, and spinel (2:1) and (4:1) $NiFe_2O_4$ MNPs showed high biomedical activities against liver carcinoma cells and non-small lung adenocarcinoma cells.

Keywords: green synthesis; magnetite; spinel $NiFe_2O_4$; star anise; co-precipitation

Citation: Al-Qasmi, N.; Almughem, F.A.; Jarallah, S.J.; Almaabadi, A. Efficient Green Synthesis of (Fe_3O_4) and ($NiFe_2O_4$) Nanoparticles Using Star Anise (*Illicium verum*) Extract and Their Biomedical Activity against Some Cancer Cells. *Materials* **2022**, *15*, 4832. https://doi.org/10.3390/ma15144832

Academic Editor: Claudio Evangelisti

Received: 22 June 2022
Accepted: 7 July 2022
Published: 11 July 2022

1. Introduction

Magnetic nanoparticles (MNPs) have been extensively investigated owing to their interesting properties, such as excellent magnetic activity, chemical and thermal stability, high surface-area-to-volume ratio, good adsorption behavior, and photocatalytic activity [1–4]. However, ferrite in the form of magnetite (Fe_3O_4), maghemite (γ-Fe_2O_3), and doped-ferrite have particularly received a large amount of attention [5–7]. Generally, based on the crystal structure, ferrite nanoparticles are classified as hexagonal ($MFe_{12}O_{19}$), garnet ($M_3Fe_5O_{12}$), or spinel (MFe_2O_4) structures, where M is a transition metal cation such as Ni, Mg, Co, Cu, or Zn [8,9]. MNPs have potential uses in a wide variety of applications based on their electrochemical and antimicrobial activity, such as organic catalysis, photocatalysis, fuel cells, electronic devices, water remediation, drug delivery, and cell therapy [10–13]. The conventional physical and chemical methods that are used to synthesize MNPs are co-precipitation, thermal decomposition, sonochemical, sol–gel, hydrothermal, and chemical combustion methods [14–17]. In recent decades, the limitations of these methods have been clarified, including long processing times, high cost, use of hazardous chemical compounds, and the release of toxic reagents into the environment [18,19].

Currently, green nanotechnology is attracting significant scientific attention owing to its high potential for addressing environmental challenges as it is inexpensive, safe, and eco-friendly [20,21]. Therefore, improved protocols for the green synthesis of MNPs

using natural extracts and microorganisms have been reported. Prokaryotes (e.g., bacteria, algae, and fungi) produce a large number of inorganic materials as by-products because of their huge biodiversity [22]. In addition, the leaves, roots, seeds, and flowers of plants contain diverse phenolic compounds that can reduce metal ions to metal nanoparticles (NPs) simply and rapidly [23,24]. Therefore, the analysis of such compounds for MNP biosynthesis may be of use more broadly for other applications as well. In addition, there is potential for MNPs to have biotechnological and medical applications [25,26].

The main purpose of the current research was to develop a green method for the synthesis of two types of MNPs: magnetite (Fe_3O_4) and spinel nickel ferrite [(2:1) and (4:1) $NiFe_2O_4$], via a simple, rapid, economical and effective co-precipitation method. Star anise (*Illicium verum*) extract was used as an eco-friendly reducing agent for the reduction of metal ions to metal nanoparticles. To the best of our knowledge, this is the first time that the preparation of magnetite Fe_3O_4, and spinel (2:1) and (4:1) $NiFe_2O_4$ MNPs using star-anise extract has been reported. The synthesized MNPs were characterized using field-emission scanning electron microscopy (FESEM), energy-dispersive X-ray spectroscopy (EDS), UV–visible spectroscopy (UV–vis), and X-ray diffraction (XRD). Once characterized, the cytotoxicity effect of the MNPs against liver carcinoma cells and non-small lung adenocarcinoma cells was examined as an example of a biomedical application.

2. Experimental Section

2.1. Chemicals

Analytical-grade iron chloride ($FeCl_3{\cdot}6H_2O$, $FeCl_2{\cdot}4H_2O$), and nickel chloride ($NiCl_2.\ 6H_2O$) were obtained from Sigma-Aldrich and used without additional purification. All chemicals and plant extracts were prepared in this investigation using double-distilled water as the solvent.

2.2. Preparation of the Star Anise Extract

Star anise (*Illicium verum*) was purchased from a local market. To prepare the extract of star anise, we used the same procedure as reported previously [27]. The extract was filtered and centrifuged at 15,000 rpm before being used for the preparation of MNPs.

2.3. Synthesis of the Magnetic Nanomaterials

Magnetite Fe_3O_4, and spinel (2:1) and (4:1) $NiFe_2O_4$ MNPs were synthesized by green co-precipitation methods. First, $FeCl_3{\cdot}6H_2O$ and $FeCl_2{\cdot}4H_2O$ with 1:2 molar proportions were dissolved in 100 mL of double-distilled water. The reaction mixture was then boiled for 10 min at 60 °C on a hot plate with vigorous stirring. Next, 10 mL of the star-anise extract was added to the reaction mixture. The color changed from light to darkish brown, indicating the production of Fe_3O_4 MNPs. Then, the solution was dried in an oven for 24 h at 80 °C. Subsequently, the obtained powder was calcined at 700 °C for 2 h [28]. Second, the spinel $NiFe_2O_4$ MNPs with (2:1) and (4:1) ratio of ($NiCl_2{\cdot}6H_2O$: $FeCl_3{\cdot}6H_2O$) were synthesized following the same above procedure.

2.4. Instrumentation and Characterization

The morphology and elemental composition of the MNPs were studied using FESEM and EDS measurements (JEOL JSM-7600 F Technologies Ltd., Raleigh, NC, USA). A Scanting XDS 2000 diffractometer equipped with a Cu Kα radiation source was used to obtain the XRD patterns of the MNPs. The spectroscopic analysis of the MNPs was performed using a UV/VIS/NIR spectrometer (Lambda 750, Parkin Elmer).

2.5. In Vitro Cytotoxicity Evaluation

In vitro cytotoxicity evaluation of the three different types of MNPs was performed against liver carcinoma cells (Hep G2, ATCC number HB-8065) and non-small lung adenocarcinoma cells (A549, ATCC number CCL-185). All cell products were purchased from the American Type Culture Collection (ATCC). Living cellular models were used between

passages 12–27. Dulbecco's modified Eagle's medium (DMEM) supplemented with 10% (*v*/*v*) fetal bovine serum (FBS), streptomycin (100 µg/mL), and penicillin (100 U/mL) were used to maintain the two cell lines.

The cellular viability of Hep G2 and A549 cells following the application of the MNPs was assessed by measuring the cellular metabolic activity using MTS assay kit (CellTiter 96 Aqueous One Solution Cell Proliferation Assay, Promega, Madison, WI, USA). Following the cell confluency, cells were detached from the flask using trypsin, then counted with the trypan blue exclusion test, and seeded at a seeding density of 1.5 × 104 cells/well into 96-well plates. The samples were then incubated overnight in a humidified 5% CO_2 cell culture incubator at 37 °C. The next day, 100 µL samples of increasing concentrations of the tested MNPs (15.62–1000 µg/mL) were incubated with the two human cancerous cell types for 24 h. The cells were incubated with only DMEM, or with Triton X-100, as the positive and negative controls, respectively. The investigated nanoparticles were aspirated from the wells, 100 µL of DMEM was added, and then 20 µL of the MTS reagent was added to each well. Thereafter, cells were covered with aluminum foil and incubated for 2–3 h at 37 °C. A Cytation 3 absorbance microplate reader (BioTek Instruments Inc., Winooski, VT, USA) was used to measure MTS absorbance at 490 nm. The percentage of viable cells was calculated using the following equation:

$$\text{Cell viability } (\%) = (\text{S} - \text{T})/(\text{H} - \text{T}) \times 100$$

where S is the absorbance of the cells treated with the MNPs, H is the absorbance of the cells treated with DMEM (positive control), and T is the absorbance of the cells treated with Triton X-100 (negative control).

3. Results and Discussion

3.1. Morphology

Figure 1a–c, Figures 2a–c and 3a–c display the FESEM images of the MNPs synthesized using the star-anise extract. Figure 1a–c shows that the magnetite Fe_3O_4 MNPs comprised irregular clusters of overlapping platelets. However, Figures 2a–c and 3a–c clearly depict the distinct pyramidal shapes of both spinel (2:1) and (4:1) $NiFe_2O_4$ MNPs. Therefore, the precursor metallic salts did not have a significant effect on the morphology of the spinel (2:1) and (4:1) $NiFe_2O_4$ MNPs. It is possible that the highly agglomerated shapes might be due to the magnetic properties of the MNPs [29]. The size of the MNPs was determined to be in the range of 0.1–1 µm.

The EDS spectra of the MNPs fabricated using star-anise extract are shown in Figures 1d, 2d and 3d. In the case of magnetite Fe_3O_4 (Figure 1d), strong signal peaks at 6.2 keV and 0.6 keV for iron and at 0.5 keV for oxygen were observed. The presence of iron and oxygen verified the formation of magnetite Fe_3O_4 MNPs [30]. Typical peaks of nickel, iron, and oxygen were noticed in the EDS spectra for the (2:1) and (4:1) spinel MNPs (Figures 2d and 3d). However, it is clear that the use of star-anise extract via simple co-precipitation forms highly crystalline Fe_3O_4, and spinel (2:1) and (4:1) $NiFe_2O_4$ MNPs.

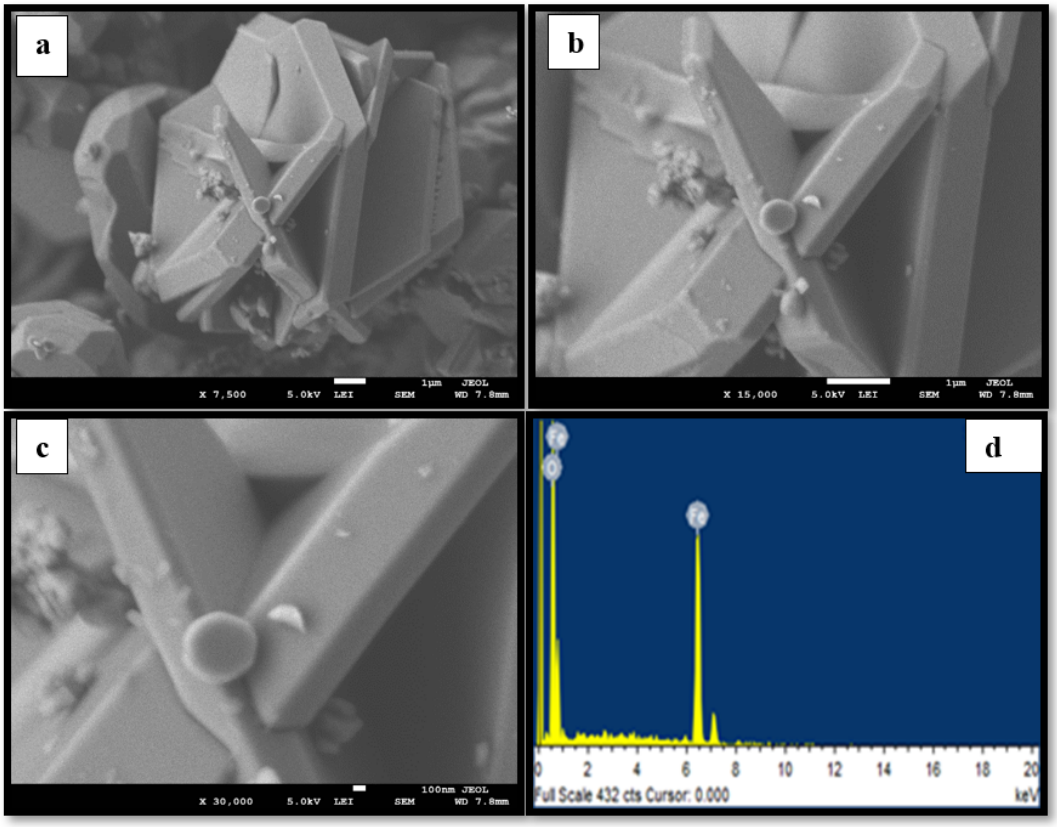

Figure 1. Representative FESEM images (**a**–**c**) at different magnifications of the synthesized Fe_3O_4 NPs and (**d**) EDS.

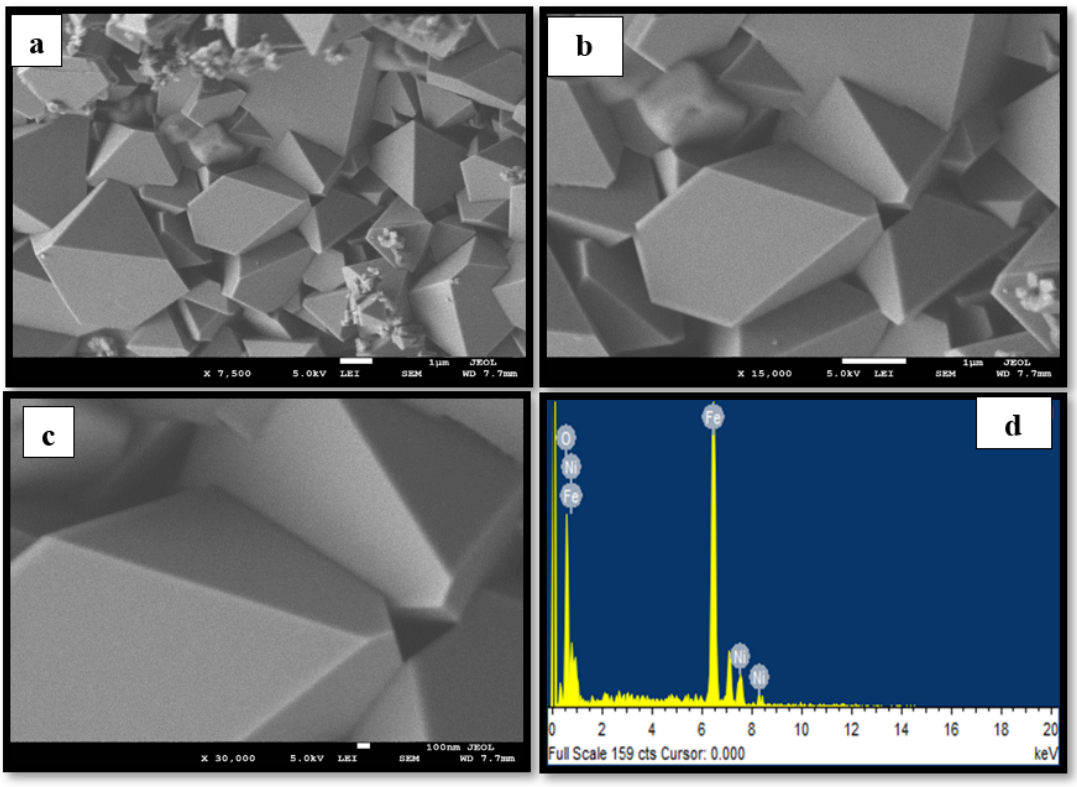

Figure 2. Representative (**a**–**c**) FESEM images at different magnifications and (**d**) EDS spectrum of the synthesized spinel (2:1) $NiFe_2O_4$ MNPs.

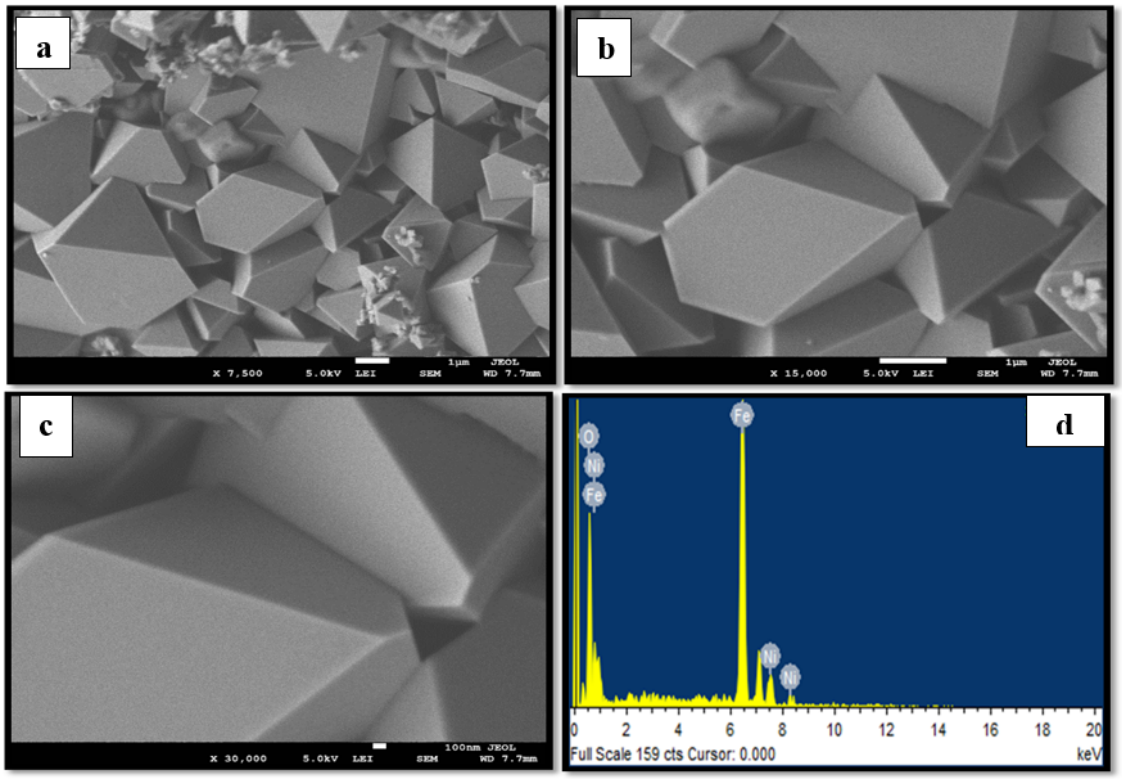

Figure 3. Representative (**a**–**c**) FESEM images at different magnifications and (**d**) EDS spectrum of the synthesized spinel (4:1) $NiFe_2O_4$ MNPs.

3.2. UV Spectra

The electronic transitions of the MNPs during the chemical reaction between the extract of star anise and precursor metallic salts were studied using UV–vis spectrophotometry in the range of 200–800 nm. The spectrum of the Fe_3O_4 MNPs has a strong peak at approximately 300–350 nm [31] (Figure 4a), while this peak shifted to ~700 nm for spinel (2:1) and (4:1) $NiFe_2O_4$ MNPs (Figure 4b) [32]. The clear absorption peaks indicate that the synthesized nanoparticles were stable and well dispersed in the solution.

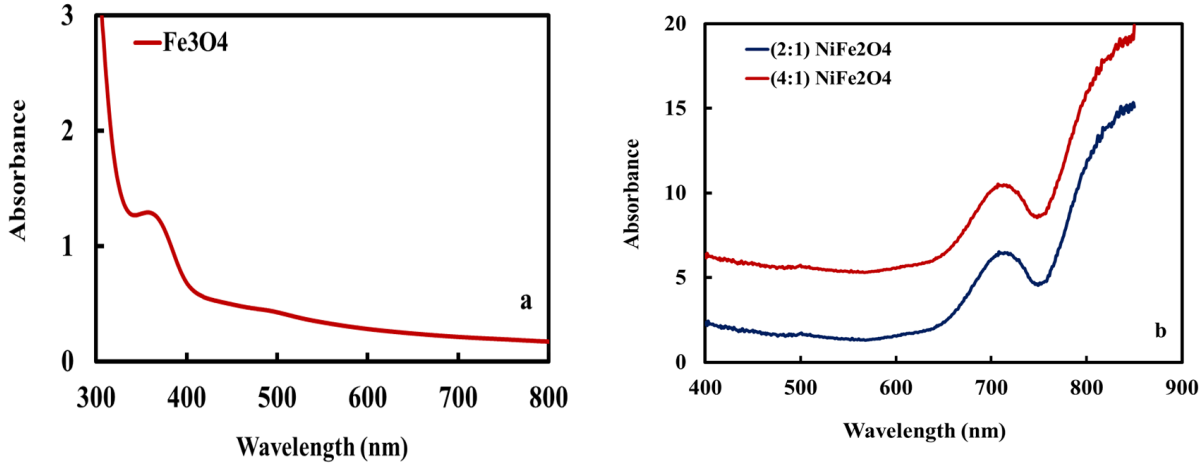

Figure 4. UV spectra of the synthesized (**a**) Fe_3O_4 and (**b**) spinel (2:1) and (4:1) $NiFe_2O_4$ MNPs.

3.3. Crystal Structure

Figure 5 displays the XRD spectra of the synthesized (a) magnetite Fe_3O_4 and (b) spinel (2:1) $NiFe_2O_4$ and (c) (4:1) $NiFe_2O_4$ MNPs. Intense reflection peaks of the synthesized

magnetite Fe_3O_4 MNPs were observed at 2θ = 30.8, 38.5, 43.7, 53.7, 56.5, and 62.5° of magnetite Fe_3O_4 [33], as shown in Figure 3a. Scherrer's equation D = 0.9λ/β cosθ was used to calculate the average crystallite size (D), where β is the full width at half maximum (FWHM) line broadening of the most intense peak, K is the Scherrer constant, θ is Bragg's angle, and λ is the X-ray wavelength. This analysis gave values of 66.8 nm.

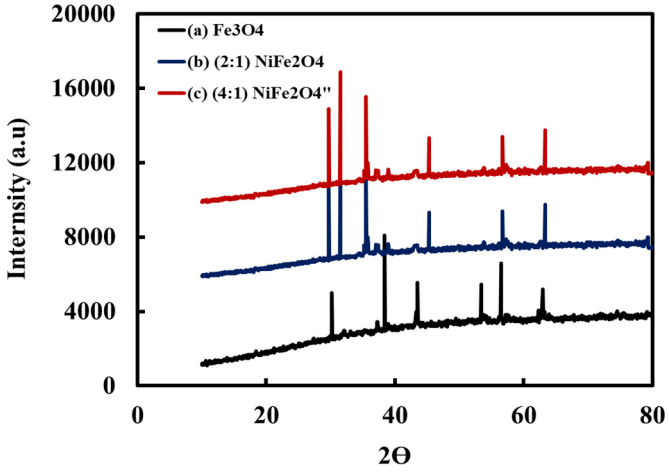

Figure 5. XRD spectra of the synthesized Fe_3O_4, and spinel (2:1) and (4:1) $NiFe_2O_4$ MNPs.

The diffraction patterns of spinel (2:1) and (4:1) $NiFe_2O_4$ MNPs are shown in Figure 5 (line a,b,c), respectively. The peaks are intense and sharp, indicating the excellent crystallinity of the synthesized MNPs. Peaks were observed at 2θ values of 29. 7, 31.5, 35.5, 45.3, 56. 7, and 63.2° of the spinel $NiFe_2O_4$ structure [34]. No additional peaks were observed, indicating that the synthesized MNPs were of high purity. In addition, the crystallite size was determined using Scherrer's formula as 72.5 and 72.9 nm.

3.4. In Vitro Cytotoxicity

The in vitro cytotoxicity assessment of the applied MNPs is an essential step toward biomedical application. In this experiment, increased concentrations of the MNPs were tested against Hep G2 and A549 cell lines to define the optimal concentrations that do not cause cytotoxic effects to living tissue and to identify the safety of MNPs for further studies.

Liver carcinoma cells were used because it is known that the liver is the main site for the metabolism for chemicals and food. Whether the medication is taken orally and then crosses the digestive system to the blood circulation system or whether it is taken by intravenous administration, it should pass through the liver. Furthermore, many chemicals should be metabolized through the liver before they are excreted. Either the chemical compound or the metabolite could be toxic to the liver. Therefore, the liver is one of the main organs that needs to be safe during the administration of any chemicals. Cancer in hepatic cells is ranked in fourth place for causing death for cancer-related deaths [35]. Moreover, the liver has a vital role in immunological reaction and inflammation due to its unique structure and function [35].

Figure 6a represents the effect of magnetite Fe_3O_4, spinel (2:1) and (4:1) $NiFe_2O_4$ NPs with different base concentrations on the cellular metabolic activity of Hep G2 cell line using MTS assay after a 24 h incubation time. The results showed high metabolic activity of all the applied nanoparticles comparable to the positive control with no observable effect of the tested nanoparticles on the cell viability. High viability of the human cancerous cells was achieved at all concentrations applied even at the maximum concentration used (1000 μg/mL). The level of viability of the highest and the lowest concentrations used was almost comparable.

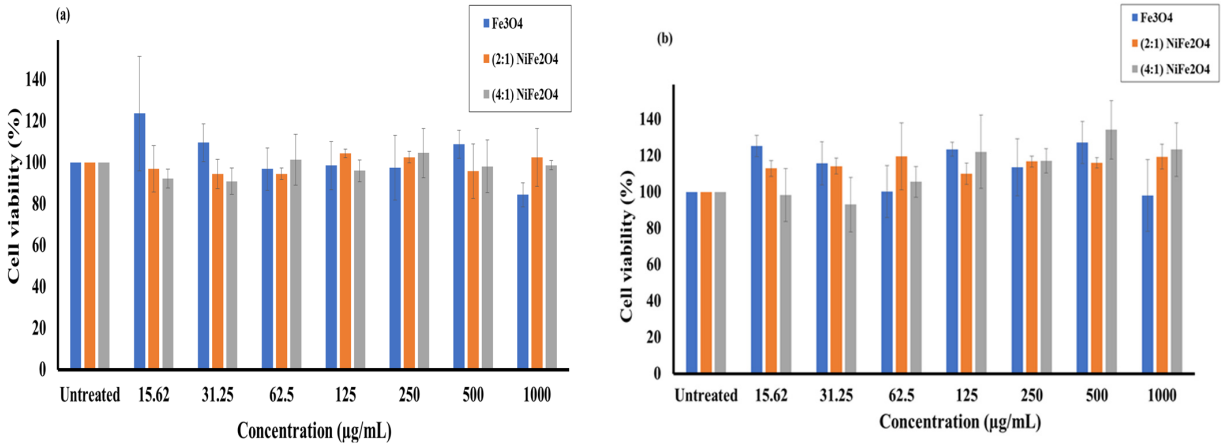

Figure 6. Cell viability of the synthesized Fe_3O_4, and spinel (2:1) and (4:1) $NiFe_2O_4$ NPs after their incubations for 24 h with (**a**) Hep G2 and (**b**) A549 cell lines. The data are the result of MTS assay expressed as cell viability (%) and presented as the mean ± SD (n = 3).

Figure 6b demonstrates the percentage of cell viability of A549 cells following the application of tested MNPs and incubation for 24 h. It should be noted that high cellular metabolic viability and low cytotoxicity were obtained at all tested concentrations in all types of nanoparticles used even at the highest concentration used (1000 µg/mL). The results showed no effect of all applied doses on the cell viability as its level was nearly similar at the lowest and highest concentration applied, 15.62 and 1000 µg/mL, respectively.

The in vitro evaluation of the magnetite Fe_3O_4, and spinel (2:1) and (4:1) $NiFe_2O_4$ NPs showed low cytotoxicity effects on Hep G2 and A549 cells for the range of concentrations determined in the MTS assay, suggesting these MNPs as a useful bio-nanomaterial for medical applications.

4. Conclusions

Using a simple, rapid, inexpensive, and green co-precipitation approach, magnetite Fe_3O_4 and spinel (2:1) and (4:1) $NiFe_2O_4$ MNPs were successfully synthesized in this study. The star anise extract was used as an environmentally friendly reducing agent instead of a highly toxic chemical reagent. According to the findings, the synthesized MNPs were found to be extremely crystalline and pure. FESEM measurements revealed that the particle sizes of the MNPs were in the range of 0.1–1 µm. Furthermore, according to XRD analysis, the sizes of the prepared MNPs were 66.8, 72.5, and 72.9, respectively. The MNPs fabricated with the star-anise extract could be used as cancer treatments due to excellent biological activity against liver cancer and non-small lung adenocarcinoma cells.

Author Contributions: Conceptualization, N.A.-Q.; Data curation, N.A.-Q.; Formal analysis, N.A.-Q.; Investigation, N.A.-Q., F.A.A. and S.J.J.; Methodology, N.A.-Q., A.A.; F.A.A. and S.J.J.; Resources, A.A.; Software, N.A.-Q.; Writing—original draft, N.A.-Q., F.A.A., S.J.J. and A.A.; Writing—review & editing, N.A.-Q. All authors have read and agreed to the published version of the manuscript.

Funding: This research received no external funding.

Institutional Review Board Statement: Not applicable.

Informed Consent Statement: Not applicable.

Data Availability Statement: Data are contained within the article.

Acknowledgments: The authors are grateful for the support of the Chemistry Department at Taif University and the Ministry of Education in the Kingdom of Saudi Arabia. The authors also gratefully acknowledge Iqbal Ismail and Mohammed Aslam from the Center of Excellence in Environmental Studies at King Abdul Aziz University for assistance with the UV–vis measurements.

Conflicts of Interest: The authors declare no conflict of interest.

References

1. Campos, E.; Denise, V.; José, I.; Elizabeth, C.; Rita, C. Synthesis, characterization and applications of iron oxide nanoparticles—A short review. *J. Aerosp. Technol. Manag.* **2015**, *7*, 267–276. [CrossRef]
2. Vedrtnam, A.; Kishor, K.; Sunil, D.; Aman, K. A comprehensive study on structure, properties, synthesis and characterization of ferrites. *AIMS Mater. Sci.* **2020**, *7*, 800–835. [CrossRef]
3. Unsoy, G.; Gunduz, U.; Oprea, O.; Ficai, D.; Sonmez, M.; Radulescu, M.; Alexie, M.; Ficai, A. Magnetite: From synthesis to applications. *Curr. Top. Med. Chem.* **2015**, *15*, 1622–1640. [CrossRef]
4. Rashdan, S.A.; Hazeem, L.J. Synthesis of spinel ferrites nanoparticles and investigating their effect on the growth of microalgae *Picochlorum* sp. *Arab. J. Basic Appl. Sci.* **2020**, *27*, 134–141. [CrossRef]
5. Klekotka, U.; Dariusz, S.; Simo, S.; Beata, K. Influence of atomic doping on thermal stability of ferrite nanoparticles—Structural and Magnetic Studies. *Materials* **2021**, *14*, 100. [CrossRef] [PubMed]
6. Kharisov, B.; Kharissova, O.; Rasika Dias, H. *Iron-Based Nanomaterials in the Catalysis*; InTech: Rijeka, Croatia, 2016; pp. 50–55.
7. Shao, H.; Yoon, T.; Liong, M. Magnetic nanoparticles for biomedical NMR-based diagnostics. *Beilstein J. Nanotechnol.* **2010**, *1*, 142–154. [CrossRef]
8. Tolani, S.C.; Golhar, A.; Rewatkar, K. A review of morphological, structural behaviour and technological applications of ferrites. *AIP Conf. Proc.* **2019**, *2104*, 030032.
9. Avval, Z.; Malekpour, L.; Raeisi, F. Introduction of magnetic and supermagnetic nanoparticles in new approach of targeting drug delivery and cancer therapy application. *Drug Metab. Rev.* **2020**, *52*, 157–184. [CrossRef]
10. Kaur, M.; Kaur, N. Ferrites: Synthesis and applications for environmental remediation, in Ferrites and Ferrates: Chemistry and Applications in Sustainable Energy and Environmental Remediation. *ACS Publ.* **2016**, 113–136. [CrossRef]
11. Sharma, J.; Pratibha, S.; Gurdip, S.; Hardev, S. Nanoferrites of transition metals and their catalytic activity. In *Solid State Phenomena*; Trans Tech Publications Ltd.: Bäch, Switzerland, 2016; Volume 241, pp. 126–138.
12. Lagashetty, A.; Pattar, A.; Ganiger, S.K. Synthesis, characterization and antibacterial study of Ag doped magnesium ferrite nanocomposite. *Heliyon* **2019**, *5*, 1760. [CrossRef]
13. Amiri, M.; Pardakhti, A.; Ahmadi-Zeidabadi, M. Magnetic nickel ferrite nanoparticles: Green synthesis by Urtica and therapeutic effect of frequency magnetic field on creating cytotoxic response in neural cell lines. *Colloids Surf. B Biointerfaces* **2018**, *172*, 244–253. [CrossRef] [PubMed]
14. Majidi, S.; Fatemeh, Z.; Samad, M.; Soleymani, M.; Akbarzadeh, A. Current methods for synthesis of magnetic nanoparticles. *Artif. Cells Nanomed. Biotechnol.* **2016**, *44*, 722–734. [CrossRef] [PubMed]
15. Kaur, R.; Abshar, H.; Nusrat, I.; Samsul, A.; Mahesh, K.; Syed Kalbe, R. Synthesis and surface engineering of magnetic nanoparticles for environmental cleanup and pesticide residue analysis: A review. *J. Sep. Sci.* **2014**, *37*, 1805–1825. [CrossRef] [PubMed]
16. Sharma, R.K.; Dutta, S.; Sharma, S.; Zboril, R.; Varma, R. Fe_3O_4 (iron oxide)-supported nanocatalysts: Synthesis, characterization and applications in coupling reactions. *Green Chem.* **2016**, *18*, 3184–3209. [CrossRef]
17. Kefeni, K.K.; Msagati, T.A.; Mamba, B.B. Ferrite nanoparticles: Synthesis, characterization and applications in electronic device. *Mater. Sci. Eng. B* **2017**, *215*, 37–55. [CrossRef]
18. Egizbek, K.; Kozlovskiy, A.; Ludzik, K.; Zdorovets, M. Stability and cytotoxicity study of $NiFe_2O_4$ nanocomposites synthesized by co-precipitation and subsequent thermal annealing. *Ceram. Int.* **2020**, *46*, 16548–16555. [CrossRef]
19. Dippong, T.; Levei, E.A.; Cadar, O. Recent advances in synthesis and applications of MFe_2O_4 (M = Co, Cu, Mn, Ni, Zn) nanoparticles. *Nanomaterials* **2021**, *11*, 1560. [CrossRef]
20. Karunakaran, G.; Jagathambal, M.; Van Minh, N. Green synthesis of $NiFe_2O_4$ spinel-structured nanoparticles using Hydrangea paniculata flower extract with excellent magnetic property. *Miner. Met. Mater. Soc.* **2018**, *70*, 1337–1343. [CrossRef]
21. Nasrollahzadeh, M.; Mohaddeseh, S.; Mohammad, S. *Green Nanotechnology, Interface Science and Technology*; Elsevier: Amsterdam, The Netherlands, 2019; pp. 145–198.
22. Purohit, J.; Chattopadhyay, A.; Singh, N. *Green synthesis of microbial nanoparticle: Approaches to application, Microbial Nanobionics*; Springer: Berlin/Heidelberg, Germany, 2019; pp. 35–60.
23. Sorbiun, M.; Shayegan Mehr, E.; Ramazan, A. Biosynthesis of metallic nanoparticles using plant extracts and evaluation of their antibacterial properties. *Nanochem. Res.* **2018**, *3*, 1–16.
24. Jagessar, R. Plant Extracts Based Nanoparticles, a Good Perspective in the Development of Drugs in Nanomedicine. *Mod. Approaches Drug Des.* **2020**, *3*, 556. [CrossRef]
25. Mollarasouli, F.; Zor, E.; Ozcelikay, G.; Ozkan, S. Magnetic nanoparticles in developing electrochemical sensors for pharmaceutical and biomedical applications. *Talanta* **2021**, *226*, 122108. [CrossRef] [PubMed]
26. Wu, K.; Su, D.; Liu, J.; Saha, R.; Wang, J. Magnetic nanoparticles in nanomedicine: A review of recent advances. *Nanotechnology* **2019**, *30*, 502003. [CrossRef] [PubMed]
27. Al-Qasmi, N. Facial eco-friendly synthesis of copper oxide nanoparticles using chia seeds extract and evaluation of its electrochemical activity. *Processes* **2021**, *9*, 2027. [CrossRef]
28. Malik, A.R.; Muhammad, H.; Muhammad, A.; Muhammad, S.; Hafeez, U.; Tuna, N.; Hijaz, A.; Shafiq, A.; Thongchai, B. Lime peel extract induced $NiFe_2O_4$ NPs: Synthesis to applications and oxidative stress mechanism for anticancer, antibiotic activity. *J. Saudi Chem. Soc.* **2022**, *26*, 101422. [CrossRef]

29. Amulya, M.; Nagaswarupab, H.; Anil, M.; Ravikumara, C.; Prashanthaa, S.; Kusumaa, K. Sonochemical synthesis of $NiFe_2O_4$ nanoparticles: Characterization and their photocatalytic and electrochemical applications. *Appl. Surf. Sci. Adv.* **2020**, *1*, 100023. [CrossRef]
30. Vázquez-Vélez, E.; Martínez, H.; Castillo, F. Degradation of Acid Red 1 Catalyzed by Peroxidase Activity of Iron Oxide Nanoparticles and Detected by SERS. *Nanomaterials* **2021**, *11*, 3044. [CrossRef]
31. Chelike, D.K.; Ananthan, A.; Joydev, A.; Pawan, K.; Koustav, S.; Senthil, A.; Thangavelua, V. Functionalized iron oxide nanoparticles conjugate of multi-anchored Schiff's base inorganic heterocyclic pendant groups: Cytotoxicity studies. *Appl. Surf. Sci.* **2020**, *501*, 143963. [CrossRef]
32. Thirupathy, C.; Cathrin, S.; Limsa, S.; Sundarama, A.; Hossam, M.; Kaviyarasucd, K. Equilibrium synthesis and magnetic properties of $BaFe_{12}O_{19}/NiFe_2O_4$ nanocomposite prepared by co precipitation method. *J. King Saud Univ.-Sci.* **2020**, *32*, 1612–1618. [CrossRef]
33. Yew, Y.; Kamyar, S.; Mikio, M.; Noriyuki, K.; Nurul, B.; Ahmad, K.; Shaza, E.; Kar, X. Green synthesis of magnetite (Fe_3O_4) nanoparticles using seaweed (*Kappaphycus alvarezii*) extract. *Nanoscale Res. Lett.* **2016**, *11*, 276. [CrossRef]
34. Khoso, W.A.; Noor, H.; Muhammad, A.; Yousuf, J. Synthesis, characterization and heavy metal removal efficiency of nickel ferrite nanoparticles (NFN's). *Sci. Rep.* **2021**, *11*, 3790. [CrossRef]
35. Patrizia, L.; Antonio, G.; Rossella, F.; Antonella, A.; Eleonora, M.; Alessio, B.; Luigi, G.; Valli, D.; Nicola, S.; Vito, R. The Evolving Role of Immune Checkpoint Inhibitors in Hepatocellular Carcinoma Treatment. *Vaccines* **2021**, *9*, 532.